Thermal conductivity of CsPbBr 3 halide perovskite: Photoacoustic measurements and molecular dynamics analysis

Andrii Kanak, Pavlo Lishchuk, Vasyl Kuryliuk, Andrey Kuzmich, David Lacroix, Yuriy Khalavka, Mykola Isaiev

Thermal conductivity of $CsPbBr_3$ halide perovskite: Photoacoustic measurements and molecular dynamics analysis

Cite as: AIP Conference Proceedings **2305**, 020006 (2020); https://doi.org/10.1063/5.0033821
Published Online: 23 November 2020

Andrii Kanak, Pavlo Lishchuk, Vasyl Kuryliuk, Andrey Kuzmich, David Lacroix, Yuriy Khalavka, and Mykola Isaiev

Thermal Conductivity of $CsPbBr_3$ Halide Perovskite: Photoacoustic Measurements and Molecular Dynamics Analysis

Andrii Kanak[1], Pavlo Lishchuk[2, a)], Vasyl Kuryliuk[2], Andrey Kuzmich[2], David Lacroix[3], Yuriy Khalavka[1], and Mykola Isaiev[3, b)]

[1] *Department of General Chemistry and Chemistry of Materials, Yuriy Fedkovych Chernivtsi National University, Kotsyubynsky 2 St., 58012, Chernivtsi, Ukraine;*
[2]*Taras Shevchenko National University of Kyiv, 64/13, Volodymyrska Street, City of Kyiv, Ukraine, 01601;*
[3]*Université de Lorraine, CNRS, LEMTA, F-54000 Nancy, France;*

[a)]*Corresponding author: pavel.lishchuk@univ.kiev.ua*
[b)]*mykola.isaiev@univ-lorraine.fr*

Abstract. The paper presents the results of thermal transport properties study of $CsPbBr_3$ perovskite at room temperature. The samples were fabricated with the use of Bridgman method. For experimental investigations, the photoacoustic method in gas-microphone configuration was used. The evaluated thermal conductivity was found to be equal 1±0.3 W/(m K). Additionally, thermal conductivity was simulated with the use of equilibrium molecular dynamics approach. The value calculated with the simulation approach was found to be equal to 0.75±0.8 W/(m K). Thus, one can state good agreements of the results of simulations and experimental ones.

1. INTRODUCTION

Halide perovskites are promising for their applications in nowadays optoelectronic [1] devices, photovoltaics [2], and photonics/polaritonics [3]. They possess low densities of carriers and traps, high carrier mobilities, high optical absorption coefficients and high luminescence efficiencies. Specifically, it was found important rise (>24 % [4]) of energy conversion efficiency for hybrid organic–inorganic halide perovskite photovoltaic cells compared to the silicon based solar cells. The remarkable optical properties, low costs, and their diversity induce the significant interest in such materials. However, such materials have low stability, and they degrade under the effect of humidity and thermal loads. Against this background, the use of all-inorganic lead halide perovskites to the production of solar cells looks promising. The most suitable for these purposes is $CsPbBr_3$. Devices based on cesium lead bromide demonstrated photovoltaic performance efficiency, comparable to that of $MAPbBr_3$-based ones but with a higher thermal and moisture stability [5]. Moreover, recent reports show a significant increase in the efficiency of $CsPbBr_3$-based solar cells [6, 7].

The study of the $CsPbBr_3$ perovskite single crystals is important also because such investigations will allow characterizing more fully the functional properties of the material as compared to other forms of this compound. Furthermore, monocrystalline silicon solar panels show much higher efficiency compared to polycrystalline panels. This indicates the prospects for the use of single-crystal material in the solar cells industry. Moreover, one needs also know the thermal conductivities of the components to simulate thermal conductivity of composites [8]. Therefore, the

Thermophysics 2020
AIP Conf. Proc. 2305, 020006-1–020006-6; https://doi.org/10.1063/5.0033821
Published by AIP Publishing. 978-0-7354-4041-8/$30.00

information regarding thermal properties of bulk material is also important for the further analysis of thermal transport in the solar cells with nanoinclusions. Specifically, this information is important to tune parameters of interatomic potentials for further consideration of the phonon scattering at the interfaces [9] and interfacial thermal resistance calculations [10, 11], which is an important source of thermal conductivity redaction in nanostructured materials [12].

During operation time, different optoelectronics and photovoltaics devices can be overheated. Such overheating can lead to arising of hotspots, that can lead to a noticeable reduction of their lifetime. The latter is crucial for halide perovskite due to its low thermal conductivity, which is reduced in more than a hundred times compared to the bulk silicon. Thus, one needs to optimize thermal transport properties of such structures to increase their stability. This is the reason why the systematical study of heat conduction from both experimental and simulation sides is essential for such materials.

From simulation point of view, molecular dynamics is versatile instrument for the study of thermal transport properties of materials with different structure and composition [12, 13]. In such simulations, the atomistic system is evaluated based on the predefine potentials. Parametrization of the potentials can be done according to the ab-initio calculations and correlation between experimental and theoretical results.

As an experimental tool, photoacoustic (PA) and photothermal (PT) methods are encouraging approaches for the study of thermal physical properties of various materials. Particularly, such methods are interesting for the study of optoelectronics/photonics system due to the possibility to follow light induced heating of the structure [12, 14].

In the paper, the thermal transport properties of halide perovskite $CsPbBr_3$ were examined with the use of photoacoustic approach in gas microphone configuration. Thermal conductivity was also simulated with the use of molecular dynamics approach. The correlations between the results of experiments and molecular dynamics simulation were stated.

2. EXPERIMENTAL DETAILS

2.1.Materials Fabrications

$CsPbBr_3$ crystal was grown by the Bridgman method which is well suited for this compound given the congruent type of melting [7, 15, 16]. First, the synthesis of perovskite was carried out by the fusion of initial materials. Specifically, CsBr (6N) and $PbBr_2$ (5N) (manufactured by Alfa Aesar) in equimolar amounts were loaded in a quartz ampoule with a diameter of 11 mm, and the air was pumped out to obtain pressure equal to 10^{-4} mbar. The ampoule was sealed and placed in a three-zone vertical furnace and then slowly heated up to 645 °C, which exceeds the melting points of both reagents. This temperature was maintained several hours to achieve homogenization of the melt and to complete the reaction between CsBr and $PbBr_2$. Thereafter, the furnace was cooled down to room temperature for 20 hours. The following step was to grow the single crystal of $CsPbBr_3$. The ampoule with the synthesized material was slowly heated up to 585 °C, and then, it was gone down with a rate of 3 mm/h into the "cold" zone of the furnace until the ingot crystallization was complete. After that, the furnace was slowly cooled down to the room temperature for 50 hours. The process of synthesis and growth of perovskite single crystal was carried out using a programmable Thermocontroller Eurotherm 3504. After cooling, the grown crystal (Fig. 1) was taken out from the ampoule and cut by the wire-cutting machine. The surface of monocrystalline samples was polished by Al_2O_3 powder with a grain size of 1 and 0.3 μm with WD-40 as a lubricant.

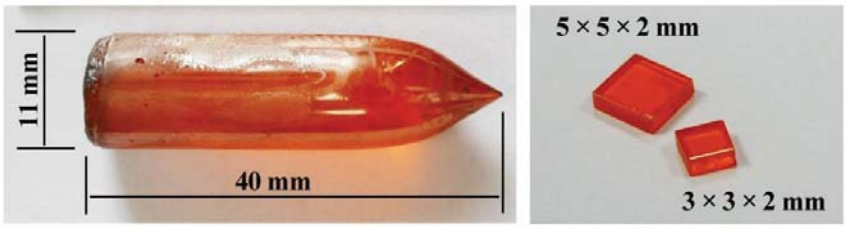

(a) (b)

FIGURE 1. a) As-grown $CsPbBr_3$ single crystal with a diameter of 11 mm; b) monocrystalline polished samples with sizes 5×5×2 mm and 3×3×2 mm

2.2.Photoacoustic Measurements

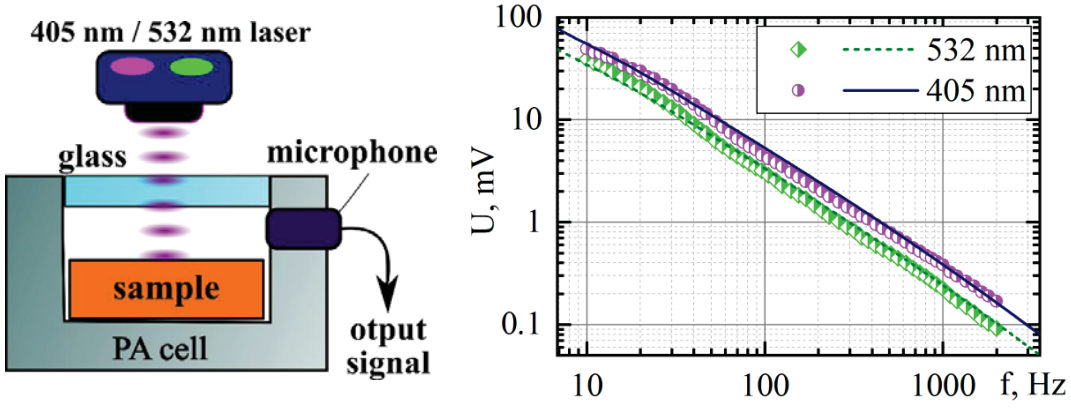

(a) (b)

FIGURE 2. a) The experimental set-up employed for thermal conductivity measurements by PA technique; b) the experimental amplitude-frequency dependences of the PA response obtained by the optical irradiation of the investigated sample by UV and green laser diodes (circles and rhombuses, respectively), approximated by model calculations (solid and dash lines, respectively)

Thermal conductivity measurements of the samples were carried out at room temperature by a photoacoustic (PA) method with gas-microphone registration in conventional configuration (see Fig. 2 a). The samples were placed inside the home-made aluminum PA cell with quartz optical transparent window and built-in commercial electret microphone. Continuous-wave single-mode green (λ = 532 nm, output optical power ~ 60 mW) and UV (λ = 405 nm, output optical power ~ 100 mW) diode lasers, modulated by a square-wave signal generator were used as non-stationary electromagnetic radiation sources. The signal obtained from the microphone was compared with the reference one from signal generator by the nanovoltmeter Unipan 232B to extract the amplitude of the informative PA signal.

The PA response was generated by the sample irradiation in the non-resonant low-frequency range from 10 Hz to 2000 Hz (see Fig. 2 b). To deduce the instrumental factors that may influence the signal formation, the experimentally obtained amplitude-frequency characteristics (AFC) were normalized at low frequencies by the calibration coefficients obtained from measurements of pure black carbon and bulk Si test samples with well-established thermal and optical properties.

The experimental AFC obtained from the $CsPbBr_3$ samples were treated by using the thermal wave approach, according to which a spatial distribution of a variable temperature component was simulated in the investigated structure under its periodical irradiation [17]. The thermal conductivity calculations of the samples were carried out numerically by minimizing the discrepancy between the experimental and simulation data based on a consideration of 1D heat conduction equation:

$$\frac{d^2T}{dz^2} - \frac{2\pi\nu c\rho i}{\kappa}T = I_0(1-R)\alpha\exp(-\alpha z), \quad (1)$$

where κ is the thermal conductivity, c is the heat capacity, ρ is the mass density of the investigated sample, f is the modulation frequency; I_0 is the incident intensity, R is the reflectivity, α is the absorption coefficient of the sample at the considered wavelength.

Pressures perturbation registered by electret microphone was evaluated based on the following equation:

$$p(f) = -T(0)\sqrt{\kappa_g/2\pi\nu c_g\rho_g i}, \quad (2)$$

where index "g" means that the considered value is taken for the gas in the PA cell.

The experimental and theoretical data for both cases (when the sample is under irradiation by green or UV laser diode) have a qualitative correlation for $CsPbBr_3$ samples when its thermal conductivity value is equal to 1 ± 0.3 W/(m K). This value is in good agreement with the results reported earlier in [18, 19].

3. MOLECULAR DYNAMICS SIMULATIONS

3.1.Thermal Conductivity Evaluation

The initial positions of the atoms (see Fig. 3) for MD simulations of thermal transport properties in $CsPbBr_3$ was taken from [16]. The interactions between atoms were set according to Buckingham and Coulomb potentials [20]. The parametrization of interactional potential was taken from [21]. For thermal conductivity calculation we used equilibrium MD approach, which is based on thermal conductivity evaluation based on the heat flux autocorrelation function:

$$\kappa_{\alpha\beta} = \frac{1}{Vk_bT^2}\int_0^\infty dt\langle J_\alpha(t)\cdot J_\beta(0)\rangle, \quad (3)$$

where V is the volume of simulation domain, k_b is the Boltzmann constant, T is the system temperature, $J_\alpha(t)$ is the heat flux in direction α at time step t.

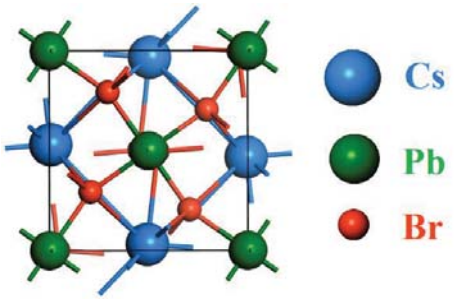

FIGURE 3. The initial positions of the atoms in the halide perovskite $CsPbBr_3$ crystalline lattice

All simulations were carried in Large-scale Atomic/Molecular Massively Parallel Simulator (LAMMPS) [22]. Before calculations of heat flux correlations with Eq. (3), the systems were equilibrated during 100 ps with the use of isothermal-isobaric (NPT) ensemble and, additionally, 100 ps in canonical (NVT) ensemble. After these steps, NVE integration during 1 ns was performed while heat fluxes in each direction was recorded. The calculations were repeated 10 times with different initial distributions of velocities, and the final value of thermal conductivity was averaged for different directions. The final evaluated value of thermal conductivity was found to be equal to 0.75±0.8 W/(m K). This value is in a good agreement with experimental results.

3.2.Vibrational density of states

Additionally, the vibrational density of states (DOS) was calculated for considered material. For the calculation, procedure described in details in [23] was used. More specifically, firstly the dynamic matrix calculations were performed based on the Green function formalism [24, 25] in the NVE ensemble with a Langevin thermostat. The systems were equilibrated during 200 ps, and then the system is run in the NVE ensemble for additional 2 ns to record the atomic displacements and velocities. Using the eigenvalues of the dynamical matrices, the phonon DOS and the phonon dispersions were then calculated using the auxiliary postprocessing code phana [25]. The evaluated DOS are presented in the Fig. 4. The calculated phonon spectrum of halide perovskite $CsPbBr_3$ is found to contain low-energy peaks, especially due to Cs and Br motion, as was well as an intrinsic dynamic instability[26].

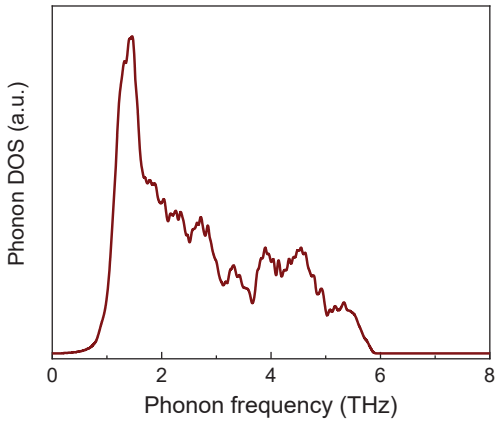

FIGURE 4. Vibrational density of states of atoms in the halide perovskite $CsPbBr_3$ crystalline lattice

CONCLUSIONS

In the paper, the features of thermal transport properties in halide perovskite $CsPbBr_3$ was considered. Firstly, thermal conductivity of material was measured with gas-microphone photoacoustic method. The photoacoustic response was excited with the use of light source with two different wavelengths to minimize impact of the optical properties. Then, thermal conductivity was evaluated with the use of equilibrium molecular dynamics approach. The good agreement was found between results of simulations and experimental ones. Our results are a basis for optimizing the thermal properties of halide perovskite for its potential applications in optoelectronic and photovoltaic devices.

ACKNOWLEDGMENTS

The publication contains the results obtained in the frames of the project ANR-19-CE09-0003. The authors thank the mesocenter EXPLOR of the Université de Lorraine and National Computing Center for Higher Education (eDari project A0080907186) for providing computational facilities. PL wants to acknowledge the financial support of the Ministry of Education and Science of Ukraine through the project “Features of photothermal and photoacoustic processes in low-dimensional silicon-based semiconductor systems” (State registration number 0118U000242). AK and YK are supported by the MESU Grant for Young Scientist (State registration number 0119U100728).

REFERENCES

1. J. Shi, W. Ge, J. Zhu, M. Saruyama, and T. Teranishi, ACS Appl. Nano Mater. (2020).
2. A. K. Jena, A. Kulkarni, and T. Miyasaka, Chem. Rev. **119**, 3036 (2019).
3. R. Su, S. Ghosh, J. Wang, S. Liu, C. Diederichs, T.C.H. Liew, and Q. Xiong, Nat. Phys. **16**, 301 (2020).
4. K. Wang, D. Yang, C. Wu, M. Sanghadasa, and S. Priya, Prog. Mater. Sci. **106**, 100580 (2019).
5. M. Kulbak, S. Gupta, N. Kedem, I. Levine, T. Bendikov, G. Hodes, and D. Cahen, J. Phys. Chem. Lett. **7**, 167 (2016).
6. X. Li, Y. Tan, H. Lai, S. Li, Y. Chen, S. Li, P. Xu, and J. Yang, ACS Appl. Mater. Interfaces **11**, 29746 (2019).
7. Y. Ding, B. He, J. Zhu, W. Zhang, G. Su, J. Duan, Y. Zhao, H. Chen, and Q. Tang, ACS Sustain. Chem. Eng. **7**, 19286 (2019).
8. A. Minnich and G. Chen, Appl. Phys. Lett. **91**, 073105 (2007).
9. S. Giaremis, J. Kioseoglou, P. Desmarchelier, A. Tanguy, M. Isaiev, I. Belabbas, P. Komninou, and K. Termentzidis, ACS Appl. Energy Mater. **3**, 2682 (2020).

10. A. T. Pham, M. Barisik, and B. Kim, Int. J. Precis. Eng. Manuf. **15**, 323 (2014).
11. Z. Wang, Mater. Today Commun. **22**, 100822 (2020).
12. K. Dubyk, L. Chepela, P. Lishchuk, A. Belarouci, D. Lacroix, and M. Isaiev, Appl. Phys. Lett. **115**, 021902 (2019).
13. I. A. Lujan-Cabrera, C. F. Ramirez-Gutierrez, J. D. Castaño-Yepes, and M. E. Rodriguez-Garcia, Phys. B Condens. Matter **560**, 133 (2019).
14. C. F. Ramirez-Gutierrez, H. D. Martinez-Hernandez, I. A. Lujan-Cabrera, and M. E. Rodriguez-García, Sci. Rep. **9**, 1 (2019).
15. J. Song, Q. Cui, J. Li, J. Xu, Y. Wang, L. Xu, J. Xue, Y. Dong, T. Tian, H. Sun, and H. Zeng, Adv. Opt. Mater. **5**, 1700157 (2017).
16. C. C. Stoumpos, C. D. Malliakas, J. A. Peters, Z. Liu, M. Sebastian, J. Im, T. C. Chasapis, A. C. Wibowo, D. Y. Chung, A. J. Freeman, B. W. Wessels, and M. G. Kanatzidis, Cryst. Growth Des. **13**, 2722 (2013).
17. P. Lishchuk, M. Isaiev, L. Osminkina, R. Burbelo, T. Nychyporuk, and V. Timoshenko, Phys. E Low-Dimensional Syst. Nanostructures **107**, 131 (2019).
18. L. Kubičár, V. Vretenár, and V. Boháč, Solid State Phenom. **138**, 3 (2008).
19. W. Lee, H. Li, A. B. Wong, D. Zhang, M. Lai, Y. Yu, Q. Kong, E. Lin, J. J. Urban, J. C. Grossman, and P. Yang, Proc. Natl. Acad. Sci. **114**, 8693 (2017).
20. S. A. Khrapak, M. Chaudhuri, and G. E. Morfill, J. Chem. Phys. **134**, 054120 (2011).
21. M. Lai, A. Obliger, D. Lu, C. S. Kley, C. G. Bischak, Q. Kong, T. Lei, L. Dou, N. S. Ginsberg, D. T. Limmer, and P. Yang, Proc. Natl. Acad. Sci. **115**, 11929 (2018).
22. S. Plimpton, J. Comput. Phys. **117**, 1 (1995).
23. V. Kuryliuk, O. Nepochatyi, P. Chantrenne, D. Lacroix, and M. Isaiev, J. Appl. Phys. **126**, 055109 (2019).
24. L. T. Kong, G. Bartels, C. Campañá, C. Denniston, and M. H. Müser, Comput. Phys. Commun. **180**, 1004 (2009).
25. L. T. Kong, Comput. Phys. Commun. **182**, 2201 (2011).
26. C. Gehrmann and D. A. Egger, Nat. Commun. **10**, (2019).